Continuous Cooling Kinetics Modeling for a Medium–High Carbon Spring Steel

He Huang ⓘ, Jinping Liu, and Baoyu Wang

Continuous cooling transformation (CCT) diagrams of steel are the basis to determine the optimum heat treatment technology. Combined with metallography, the CCT diagram of medium–high carbon spring steel 60Si2CrA was obtained by dilatometric measurement at cooling rates from 0.5 to 50 K/s. It is found that ferrite, pearlite, and martensite were available in the experimental range. Taking into account of the incubation time and volume fraction evolution of the new phase, a new phase transformation kinetics model is established to estimate the fraction of ferrite and pearlite during continuous cooling process (CCP). Material constants in the model were determined and optimized by minimizing the errors between experimental and predicted data. The kinetics model was validated and proved its efficiency in predicting the new phase fraction of 60Si2CrA during continuous cooling and will probably constitute a useful tool for guiding the production process.

1. Introduction

The medium–high carbon spring steel 60Si2CrA is widely used in making grinding balls. As main grinding media in ball mills, grinding balls are extensively employed in many industries, such as the mineral process. The wear performance of grinding balls is related to heat treatment process. Time–temperature transformation (TTT) and continuous cooling transformation (CCT) diagrams are two basic transformation diagrams, which are not only important bases of establishing reasonable heat treatment process, but also the essential foundation of the solid-state phase transformation theory. Compared with TTT diagrams, CCT diagrams are generally closer to engineering conditions (Ref 1). Therefore, understanding of the relationship between cooling rates and the degree of phase transformation in 60Si2CrA steel in continuous cooling process (CCP) is crucial to the mechanical properties of grinding balls.

Numerous attempts have been made to obtain the CCT curves. CCT diagrams can be converted from existing TTT diagrams using Scheil's additivity rule. For example, Zhang et al. (Ref 2) calculated partial CCT curve of a plain carbon steel in accordance with the Avrami equation and Scheil's additivity rule. Calculation methods using artificial intelligence methods provide an alternative choice. Wang et al. (Ref 3) and Trzaska et al. (Ref 4) developed artificial neural network (ANN) models to predict CCT diagrams based on assumed

chemical compositions and austenitizing temperature. In the absence of the literature data, the CCT diagram is usually obtained by dilatometric measurement combined with some other methods, such as metallographic analysis, hardness tests, and differential scanning calorimetry method.

Many researchers have studied the continuous cooling behavior of medium–high carbon steel. Gao (Ref 5) measured the CCT curve of 60Si2CrVA, and the critical cooling rate for full martensite is 5.3 K/s. Huang et al. (Ref 6) studied the CCT curves, structure, and phase transformation of 60Si2CrVAT at different finishing rolling temperature and cooling rates. Wu et al. (Ref 7) concluded that with the increase in niobium content in 60Si2CrVAT, the high-temperature and medium-temperature transitions in CCP were promoted. Yu et al. (Ref 8) came to the conclusion that to obtain a great quantity of sorbate for 65Mn steel, the cooling rate should be between 1 and 3 K/s using the CCT diagram. Deng et al. (Ref 9) obtained the CCT diagram of 70Mn, which is usually used for forging grinding balls, and the relationships between phase transformation points/volume fraction and cooling rate were built by regression calculation. Using DIL805A dilatometer with microstructure and hardness measurement, Chen et al. (Ref 10) found that the martensite transformation start temperature of 60Si2CrA steel is 502 K, and that austenite mainly decomposed into pearlite and martensite in the applied cooling rate range from 1 to 30 K/s. Experiments conducted by Jiang et al. (Ref 11) showed that with the increase in quenching rates from 10 to 800 K/s, strength, plasticity, and hardness of 60Si2CrVAT increase to a peak, while martensite transformation start temperature shows the opposite characteristics. Phase transformation models in CCP suitable for further computer simulation were not established in the aforementioned studies. Thus, it makes sense to establish an appropriate phase transformation model for 60Si2CrA steel to predict supercooled austenite decomposition during CCP.

Researchers have developed various phase transformation models during CCP from supercooled austenite. Based on the Avrami-type equation and additivity rule, Suehiro et al. (Ref 12) developed a mathematical model for high carbon steel, which can be used to calculate the progress of transformation in

He Huang, Jinping Liu, and Baoyu Wang, School of Mechanical Engineering, University of Science and Technology Beijing, Beijing 100083, China; and Beijing Key Laboratory of Lightweight Metalforming, Beijing 100083, China. Contact e-mails: huanghe91@yeah.net, liujp@ustb.edu.cn and bywang@ustb.edu.cn.

an arbitrary cooling practice. Quidort and Brechet (Ref 13) presented a kinetics model applicable to the transformation from austenite to bainite of a hypoeutectoid steel, and nucleation and growth equations in the model are included in a Kolmogorov–Johnson–Mehl–Avrami analysis. According to thirteen determined CCT diagrams of dual-phase steels, Colla et al. (Ref 14) established an ANN model to predict the fractions of ferrite, bainite, and martensite during CCP. Utilizing internal state variable (ISV) method, Yang et al. (Ref 15) and Li et al. (Ref 16) proposed a set of unified constitutive equations to forecast the new phase fraction during CCP of DIN SAE 5140 steel and boron steel, respectively.

This work aims to develop a new set of phase transformation equations to predict supercooled austenite decomposition kinetics during CCP of medium–high carbon steel 60Si2CrA. The paper is organized as follows: First, continuous cooling behavior and microstructure evolution of 60Si2CrA were investigated using dilatometry and metallography examination. Then, a kinetics model, taking into account of the incubation time and volume fraction of new phase, was proposed to predict the transformed fraction of the new phase during continuous cooling. A genetic algorithm (GA)-based optimization method was utilized to calibrate the proposed model by minimizing the errors between experimental and predicted data. Finally, comparisons between simulated and experimental fractions validated its feasibility and accuracy, and evolution of ISVs was discussed.

2. Experiments

2.1 Experimental Procedure

The chemical composition of the investigated material 60Si2CrA is Fe-0.61C-1.75Si-0.70Mn-0.83Cr-0.01Ni-0.018P-0.018S. Dilatometric experiments were performed on a quenching dilatometer DIL805A made by Bahr-Thermoanalyse Gmbh, and the resolution $\Delta L/K$ of the dilatometer is 0.05 μm/K. Cylindrical test specimens with a diameter of 4 mm and a length of 10 mm were used for this study.
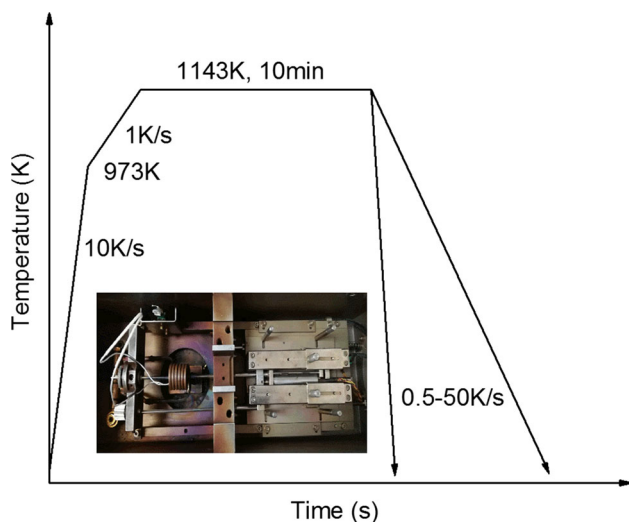

Fig. 1 Temperature profile and testing procedure of dilatometric experiments

Figure 1 shows the temperature profile and testing procedure. Specimens were inductively heated under vacuum to 973 K at a heating rate of 10 K/s to save time and then heated to 1143 K at a rate of 1 K/s. After isothermal soaking at 1143 K for 10 min, specimens were quenched by nitrogen to room temperature at a rate of 0.5, 1, 2, 3, 4, 5, 6, 7, 8, 9, 10, 30, or 50 K/s. Specimens were sectioned along the longitudinal axis and then polished and chemically etched with 4% nitrate alcohol solution to reveal the microstructure using an optical microscope after CCP. In this study, the start time of the CCP is set as the time origin.

2.2 Experimental CCT Curve

Dilation curves at the cooling rates of 0.5, 2, 3, 5, and 9 K/s in CCP are presented in Fig. 2. The resulting structure is a mixture of ferrite and pearlite (F + P) at the heating rates ranging from 0.5 to 2 K/s. According to the previous research on 60Si2CrA (Ref 10), the resulting structure is pearlite + martensite or martensite when the cooling rate is greater than or equal to 3 K/s. That is to say, ferrite does not coexist with martensite in regard with CCP of 60Si2CrA, and this phenomenon also occurs in the CCT diagrams of 65Mn (Ref 8) and 70Mn (Ref 9). When the cooling rate is at the range of 3 ~ 5 K/s, martensite transformation occurred after the P transformation. When the cooling rate is 5 K/s in Fig. 2, the P transformation can be found but not obvious. With the further increase in the cooling rate, only martensite transformation is found. That is to say, the critical cooling rate to obtain microstructure without P is 6 K/s.

Figure 3 shows the microstructure of 60Si2CrA steel using an optical microscope at cooling rates of 0.5, 2, 3, 4, 5, and 6 K/s. In Fig. 3(a) and (b), the black block is P, and the white F. It can be seen that the proportion of ferrite decreases with the increase in the cooling rate. In Fig. 3(c)-(f), the black block is P, the white or gray zone is martensite (the mixed tissue of martensite and residual austenite), and the proportion of P decreases with the increase in the cooling speed. At the cooling rate of 6 K/s, P basically disappears, and the microstructure can be considered as full martensite. Dilatometric measurement and metallographic analysis are consistent with each other.

The average martensite transformation start temperature, Ms, obtained by the dilation curves is 503 K, which is
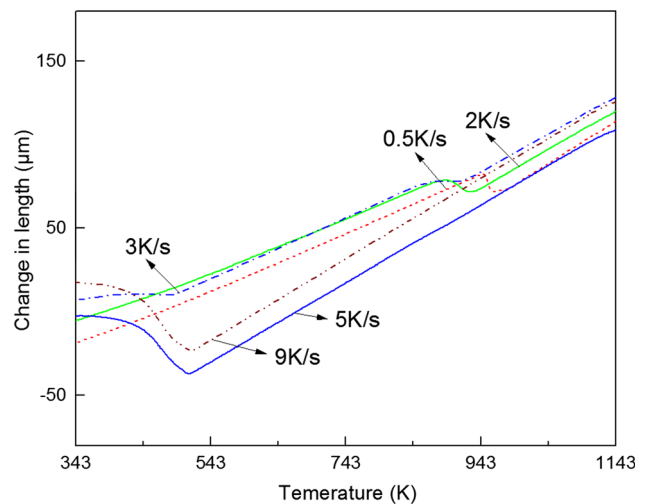

Fig. 2 Partial dilation curves of 60Si2CrA steel during cooling
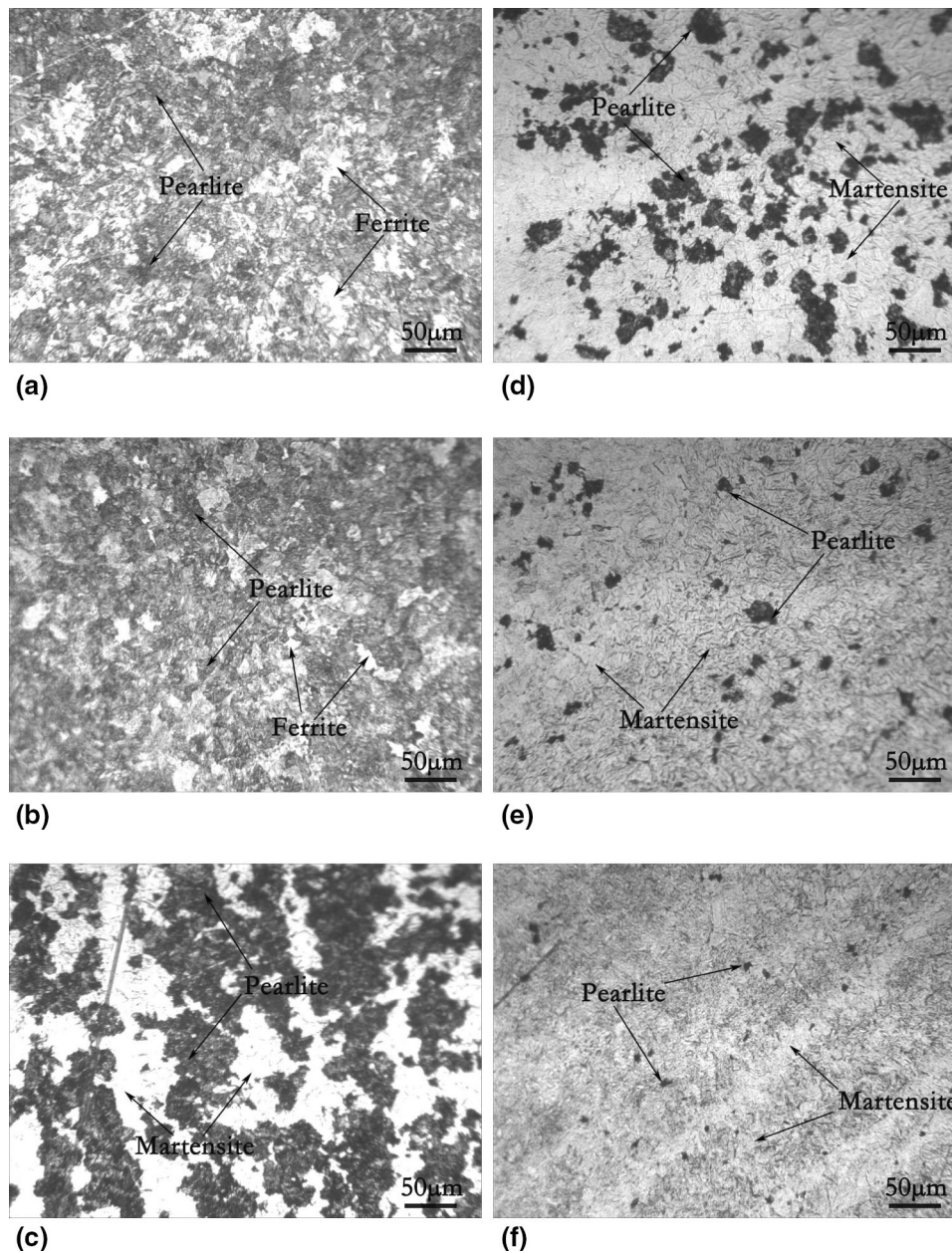
Fig. 3 Microstructure of 60Si2CrA steel at cooling rates of (a) 0.5, (b) 2, (c) 3, (d) 4, (e) 5, and (f) 6 K/s

consistent with the temperature 502 K in Reference (Ref 10). And the equilibrium temperature of austenitization start ($Ac1$) and end ($Ac3$) is estimated by the empirical formulas in Eq 1-2 (Ref 17) to be 1057.3 K and 1089.4 K, respectively.

$$A_{c1} = 1000 - 16.9w(\text{Ni}) + 29.1w(\text{Si}) - 10.7w(\text{Mn}) + 16.9w(\text{Cr}), \qquad \text{(Eq 1)}$$

$$A_{c3} = 1183 - 20.3\sqrt{w(C)} + 44.7w(\text{Si}) - 15.2w(\text{Ni}) - 30w(\text{Mn}) + 11w(\text{Cr}) - 700w(\text{P}), \qquad \text{(Eq 2)}$$

In Eq 1-2, $Ac1$ and $Ac3$ are in Kelvin, and $w()$ means the mass percent of a specific element, for example $w(C)$ equals 0.61.

It is difficult to determine the pearlite start temperature for F + P transformation conditions from the dilation curves, so ferrite and pearlite are considered as one phase when the rate is less than or equal to 3 K/s. Based on the dilation curves and metallography, the beginning and finishing transformation temperatures of each phase were determined. Then, the CCT diagram of 60Si2CrA steel was obtained as shown in Fig. 4. It is evident from Fig. 4 that ferrite + pearlite, pearlite, and martensite transition zones are in the CCT diagram, while the bainite transition zone is not. This phenomenon also occurs in the CCT diagrams of 70Mn (Fe-0.72C-0.24Si-1.09Mn) (Ref 9) and 65Mn (Fe-0.66C-0.35Si-1.05Mn) (Ref 8). The reasons are as follows. On the one hand, the alloy element manganese can form weak carbides and reduces the nucleation rate and growth rate of bainite, which retards bainite transformation (Ref 8). On the other hand, the element silicon strongly hinders the formation of carbides in the case of bainite transition, promotes the enrichment of carbon in the unconverted austenite and significantly delays the formation of bainite. Meanwhile, the

element vanadium is a strong carbides forming element, which can explain the appearance of bainite transition in CCT diagrams of 60Si2CrV (Fe-0.6C-1.5Si-0.6Mn-1.2Cr-0.16 V) in References (Ref 6-8). Due to the absence of both ferrite and bainite when martensite transition occurs, Ms temperature basically does not change in Fig. 2 and 4.

2.3 Volume Fraction of Ferrite and Pearlite

The final volume fraction of the new phase (i.e., F + P), φ_{max}, at a specific cooling rate is measured by image analysis using the software Image-Pro Plus made by Media Cybernetics Company in America. As shown in Fig. 5, when φ_{max} is mentioned, the fraction of ferrite can be zero.

The actual volume fraction of transformed F + P, φ, at a given time t is calculated by the following equation (Ref 13):

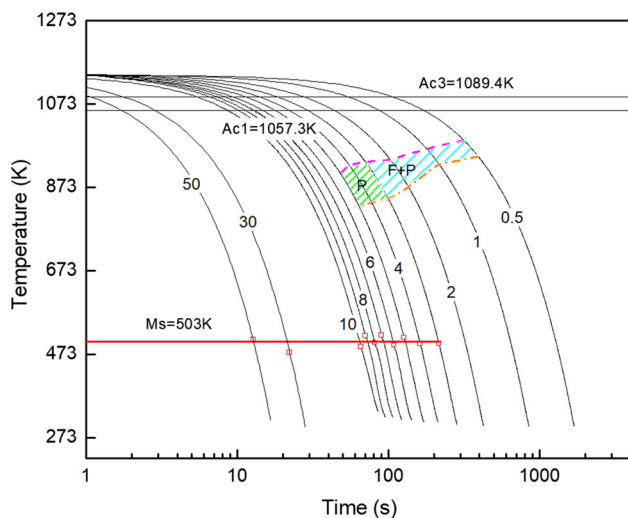$$\frac{\varphi(t)}{\varphi_{max}} = \frac{L(t) - L_0}{L_f - L_0}, \qquad (Eq\ 3)$$
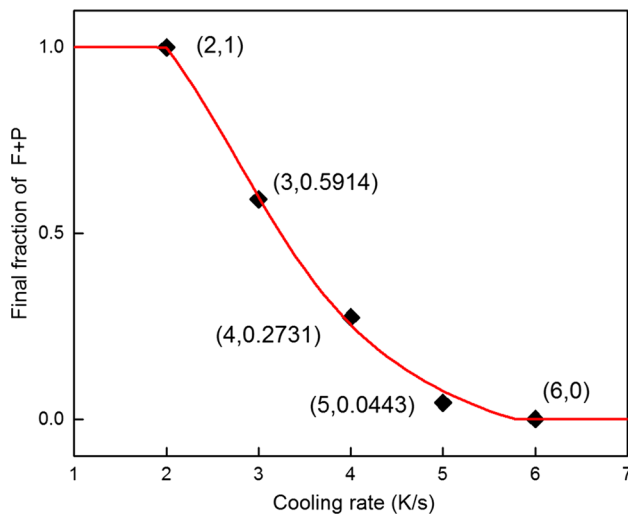

Fig. 4 CCT diagram of 60Si2CrA steel

In Eq 3, $L(t)$, L_0 and L_f are the lengths of the specimen at the given time t, before and after the completion of the CCP, respectively. The left-hand side of the equation is called the normalized volume fraction φ_n. The final volume fraction φ_{max} with cooling rate $\dot{T}$ can be phenomenally described as (Ref 18):

$$\varphi_{max} = a_1 \arctan(a_2|\dot{T}| + a_3) + a_4, \qquad (Eq\ 4)$$

where a_1, a_2, a_3, and a_4 are material parameters. The four parameters are determined using a genetic algorithm (GA)-based optimization, and the optimization procedure is similar to the calibration section. The determined values are: $a_1 = -0.6059$, $a_2 = 0.7158$, $a_3 = -1.9998$, and $a_4 = 0.6857$. The final volume fraction φ_{max} with cooling rate is given in Fig. 5, and good agreement is obtained between the computed curve and experimental data.

Figure 6 shows the evolution of the actual volume fraction of ferrite and pearlite of 60Si2CrA steel in CCP. We can see from the figure that with the increase in the cooling rate, both the start and finish transformation temperatures of F + P decrease.

3. Kinetics Modeling

3.1 Model Sketch

In light of the theory of free energy change (Ref 19) and the authors' previous study on austenite formation (Ref 20), a brief sketch of the phase transformation model to be proposed is illustrated in Fig. 7.

The CCP begins at the time t_0 ($t_0 = 0$), and the corresponding temperature is represented as T_0. Current temperature and time are expressed as T and t, respectively. When T decreases to T_c ($t = t_1$), the incubation time starts. Before the time t_1, the value of x is 0. The incubation does not come to an end until the new particle radius r reaches the critical radius r^* ($t = t^*$, $T = T^*$). The period during t^* and t_2 when the fraction of new phase φ firstly reaches φ_{max} is called the transition period. Before the time t^*, the value of φ maintains 0.

Here, we employ a parameter x ranging from 0 ($t \leq t_1$) to 1 ($t \geq t^*$) to represent the incubation time. When $t > t^*$, the
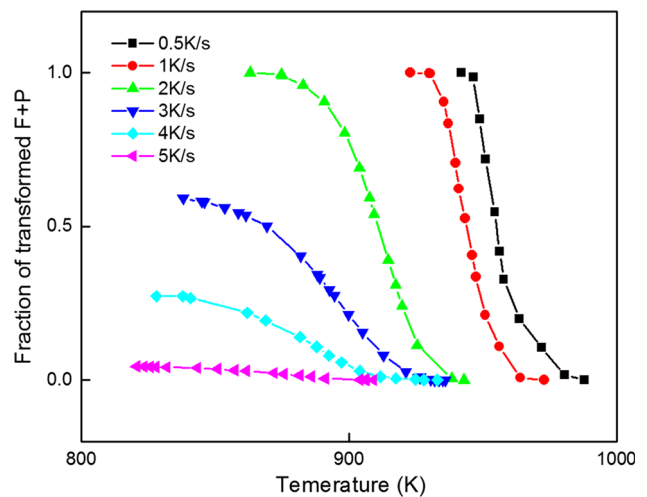

Fig. 5 Final volume fraction of ferrite and pearlite during cooling progress of 60Si2CrA steel

Fig. 6 Evolution of the volume fraction of ferrite and pearlite of 60Si2CrA steel in CCP
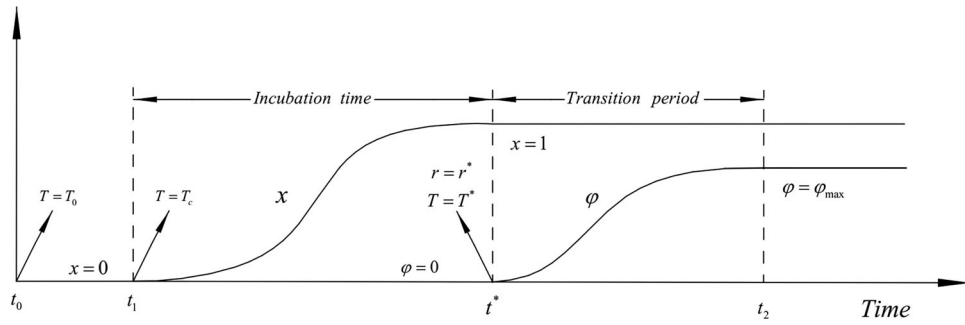
Fig. 7 Sketch of the phase transformation model in light of free energy change theory
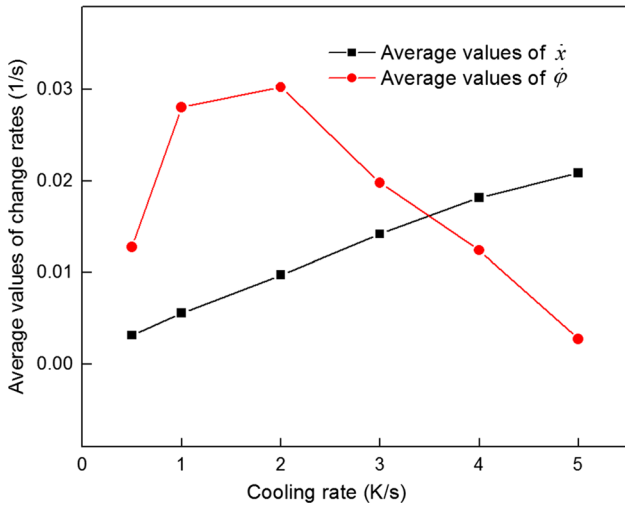

Fig. 8 Relation between average values of $\dot{x}$ (square) and $\dot{\varphi}$ (circle) and cooling rates for 60Si2CrA

difference between T_c and current temperature T is the so-called undercooling. If the time exceeds t_2, the new phase transition is completed and another phase transition may happen.

3.2 Modeling of the Incubation Period

The cooling rate in this study is expressed as $|\dot{T}|$, though the cooling rate is negative in the mathematical sense. The introduced parameter x is related to the cooling rate $|\dot{T}|$, current temperature T, and current value of x. With the increase in $|\dot{T}|$, the time between t_1 and t^* decreases, i.e., $\dot{x}$ increases. As shown in Fig. 8, the average value of $\dot{x}$ during the incubation period, which equals 1 divided by $(t_1 - t^*)$, is almost linear with cooling rates. According to the physical meaning of T_c, the incubation period does not begin before the temperature is lower than T_c. When the influences of $|\dot{T}|$, T, and x are considered, the ratio of the parameter x to the time t is described as:

$$\dot{x} = B_1(1-x)^{B_2}|\dot{T}|^{B_3}\langle 1 - T/T_c\rangle^{B_4}, \tag{Eq 5}$$

In Eq 5, B_1, B_2, B_3, and B_4 are material constants. The value of x is restricted to be between 0 and 1 by the term $(1-x)^{B_2}$. $\langle\rangle$ are Macaulay brackets. T_c equals $Ac1$ when the new phase is ferrite. And for pearlite, T_c equals $Ac3$. The value of T_c is equal to Bs (temperature below which bainite can form during CCP) in case of bainite. For ferrite and pearlite transformation in CCP

of 60Si2CrA steel, the value of T_c for F + P needs to be determined.

3.3 Modeling of the Transition Period

When the incubation time ends, the transition period initiates. In Eq 6, T^* is the temperature at the critical point $(t = t^*, r = r^*)$ where $x_- < 1$, and $x = 1$ as shown in Fig. 8.

$$T = T^*|x_- < 1, x = 1, \tag{Eq 6}$$

During the transition period, the relationship between the fraction of new phase φ and cooling rates is relatively complicated. The average value of $\dot{\varphi}$ during the transition time equals φ_{max} divided by $(t_2 - t^*)$. As shown in Fig. 8, for 60Si2CrA, the average value of $\dot{\varphi}$ rises at the beginning and then reduces with the increase in cooling rates. This trend can be expressed using a modified Gaussian-type term similar to that in Reference (Ref 19). In order to simplify the expression, evolution of φ_n for 60Si2CrA can be expressed as follows:

$$\dot{\varphi}_n = C_1\langle 1 - T/T^*\rangle^{C_2}(1 - \varphi_n)^{C_3}, \tag{Eq 7}$$

In Eq 7, C_1, C_2, and C_3 are material constants; $\langle 1 - T/T^*\rangle^{C_2}$ is introduced to describe the influence of current temperature on the new phase volume fraction explicitly and the effect of cooling rates implicitly; the term $(1 - \varphi_n)^{C_3}$ allows the value of φ_n to vary between 0 and 1, inclusively.

Then, the actual volume fraction φ can be obtained by:

$$\dot{\varphi} = \varphi_{max}\dot{\varphi}_n, \tag{Eq 8}$$

A set of phase transformation equations for 60Si2CrA steel during CCP, Eq 6-8, are established. Material constants in the model are positive and temperature independent.

4. Model Calibration

A GA-based optimization is utilized to calibrate and optimize material constants by minimizing the errors between experimental and predicted data. The volume fraction of ferrite and pearlite at the cooling rates of 0.5, 1, 2, and 5 K/s is utilized to optimize the material constants. The objective function takes the forms as follows:

$$f(X) = \frac{1}{M}\sum_{j=1}^{M}\left\{\frac{1}{N}\sum_{i=1}^{N}\left(\ln\frac{\varphi_{ij}^c + 0.5\varphi_{max}}{\varphi_{ij}^e + 0.5\varphi_{max}}\right)^2\right\}, \tag{Eq 9}$$

In Eq 9, X ($X = [B_1, B_2, B_3, B_4, T_c, C_1, C_2, C_3]$) represents the material constants required to be determined. M is the number of curves used in the optimization ($M = 4$), and N is the number of data points at a given cooling rate ($N = 38$). φ_{ij}^c and φ_{ij}^e are the computational and experimental volume fractions for the same temperature level i and cooling rate j, respectively.

The calculated incubation time parameter x and new phase volume fraction φ are numerically integrated using the forward Euler method with a constant integral step. The model contains a set of ordinary differential equations in terms of time t, so the initial values of the variables are needed. At $t = 0$, x and φ are equal to 0. The parameters of genetic algorithm here are as follows: population size = 200, crossover rate = 0.8, number of generations = 5000, mutation rate = 0.02, initial population of $X = [1e3, 1, 1, 1, 1089.4, 1e1, 1, 1]$, and bounds of $X = [0, 0, 0, 0, 1000, 0, 0, 0; 2e3, 10, 10, 10, 1200, 1e2, 10, 10]$. For ferrite and pearlite transformation in CCP of 60Si2CrA steel, T_c equals 1101.9420 K.

The determined eight values of material constants in Eq 5 and 7 are listed in Table 1.

5. Validation and Discussion

5.1 Model Validation

The predicted curves (curves) with experimental volume fractions (symbols) at the cooling rates of 0.5, 1, 3, and 5 K/s are plotted in Fig. 9. In order to verify the proposed phase transformation equations for CCP, comparisons between the predicted and experimental results at cooling rates of 2 and 4 K/s were also made. Because the final volume fractions at cooling rates ranging from 4 to 5 K/s are relatively small as shown in Fig. 4 and 5, the normalized volume fraction is adopted in Fig. 9 so that the comparisons will be more manifest. We can see that good agreement between the experimental and measured data is obtained.

5.2 Evolution of ISVs

Evolution of ISVs (including incubation parameter x, normalized fraction φ_n, and the corresponding rates dx/dt and $d\varphi_n/dt$) at cooling rates of 2, 3, and 5 K/s are predicted using the proposed model and illustrated in Fig. 10. Taking the cooling rate of 3 K/s as an example, the physical meaning of the model is explained as follows. The initial temperature is 1143 K, and the initial time $t_0 = 0$. The incubation time begins at t_1 (approximately 20 s), and the temperature equals T_c (1101.9420 K). Then, the incubation parameter x rises from 0 to 1 gradually, and the rate of which increases to a peak and

decreases to 0. When the parameter x becomes 1 for the first time, the critical time t^* (approximately 70 s) is up and the cooling degree ($T_c - T_0$) is satisfied for the occurrence of a new phase. That is to say, the transition period starts. With the increase in time from t^*, the normalized fraction rate $d\varphi_n/dt$ firstly increases and then reduces to 0, and the transition period ends when the normalized fraction progressively increases to 1 at the time t_2 (approximately 105 s).

The effect of cooling rates in the investigated range on ISVs evolution is remarkable as presented in Fig. 10. Though the required cooling degree and the phase transformation temperature are bigger with the increase in the cooling rate, the corresponding time which equals the cooling degree divided by
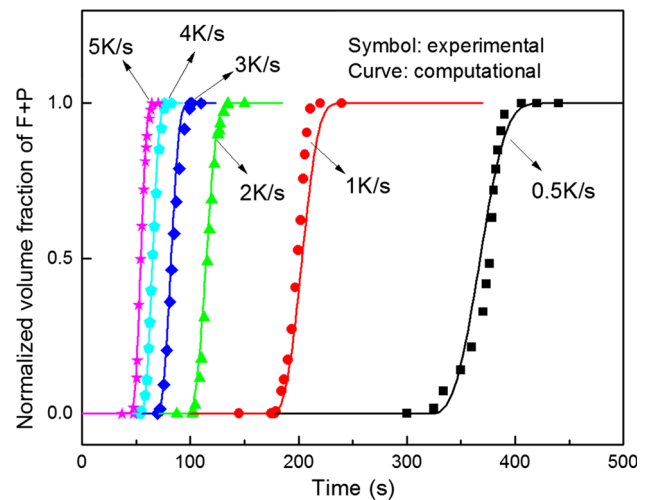

Fig. 9 Comparison of the predicted (curves) and experimental (symbols) volume fractions at all test conditions
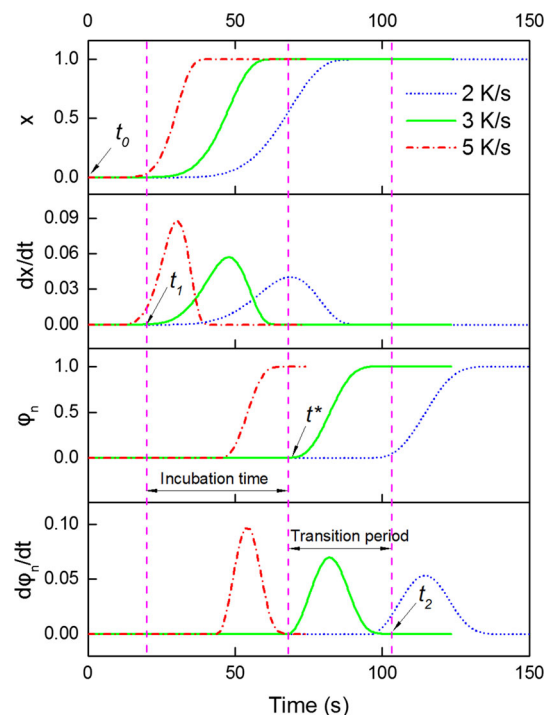

Fig. 10 Evolution of predicted ISVs with time at cooling rates of 2, 3, and 5 K/s

Table 1 Calibrated constants for the proposed model

Material constant	Determined value
$B_1(1/K)$	1230.3600
$B_2(-)$	0.8568
$B_3(-)$	0.2540
$B_4(-)$	4.0033
$T_c(K)$	1101.9420
$C_1(1/K)$	29.8540
$C_2(-)$	1.7507
$C_3(-)$	0.9177

the cooling speed decreases. That is to say, it takes less time for x to reach the saturation value 1 for a larger cooling rate. Thus, the maximum value of x growth rate is also larger. A similar law is presented for φ_n and $d\varphi_n/dt$ at different cooling rates, because the transition period is shorter at a lager cooling rate.

The above confirms the feasibility of the proposed model to characterize the phase transformation and the possibility of applying to industrial production during CCP of 60Si2CrA steel. Because the proposed phase transformation model for CCP is physically based, the model can probably be applied to other hypoeutectoid steel, and values of eight constants can be solved using genetic algorithm with the initial values in Table 1.

6. Conclusions

A set of equations have been developed to describe the phase transformation kinetics during CCP for hypoeutectoid steel 60Si2CrA. The following conclusions are obtained.

(1) The CCT diagram of the investigated 60Si2CrA was obtained using dilatometric measurement and metallographic analysis. Ferrite and pearlite (F + P) are assumed to be one, and bainite is not available in the experimental range.
(2) In light of the theory of free energy change and the authors' previous study on austenite formation, and based on the experimental data, a set of kinetics equations considering the incubation time and transition period are proposed to describe the phase transformation during CCP of 60Si2CrA.
(3) A GA-based optimization was used to calibrate material constants by minimizing the errors between experimental and predicted data, and the forward Euler method with a constant integral step was employed.
(4) The good agreement between simulated and experimental results proves both the validity of the proposed model to predict the phase transformation and the potential for application to industrial production during CCP of 60Si2CrA steel. The proposed phase transformation model for CCP is physically based and can probably be applied to other hypoeutectoid steel.

References

1. G. Xu, L. Wan, S. Yu, L. Liu, and F. Luo, A New Method for Accurate Plotting Continuous Cooling Transformation Curves, *Mater. Lett.*, 2008, **62**(2), p 3978–3980
2. Y. Zhang, D. Li, and Y. Li, Modeling of Austenite Decomposition in Plain Carbon Steels During Hot Rolling, *J. Mater. Process. Technol.*, 2006, **171**(2), p 175–179
3. J. Wang, P.J.V.D. Wolk, and S.V.D. Zwaag, Effects of Carbon Concentration and Cooling Rate on Continuous Cooling Transformations Predicted by Artificial Neural Network, *ISIJ Int.*, 2007, **39**(10), p 1038–1046
4. J. Trzaska, A. Jagiełło, and L.A. Dobrzański, The Calculation of CCT Diagrams for Engineering Steels, *Arch. Mater. Sci. Eng.*, 2009, **39**(1), p 13–20
5. H.J. Gao, Time Temperature Transformation and Continuous Cooling Transformation of Alloy Spring Steel 60Si2CrVA, *Spec. Steel*, 2003, **24**(6), p 23–24 (in Chinese)
6. X.Q. Huang, Y.Z. Liu, and J. Cui, Thermal Simulation Study on Controlled Rolling and Cooling Process for Quality Spring 60Si2Cr-VAT, *Spec. Steel*, 2007, **28**(6), p 21–23 (in Chinese)
7. H.L. Wu, F.M. Wang, C.R. Li, Q. Yan, and B. Zhang, Continuous Cooling Transformation of Under-cooled Austenite for Nb-V Microalloyed Spring Steel 60Si2CrVAT, *J. Univ. Sci. Technol. Bj*, 2011, **33**(12), p 1463–1470 (in Chinese)
8. W.H. Yu, L.T. Xu, Y.J. Zhang, H.F. Wang, J.T. Han, and J. Liu, Characteristic of 65Mn Steel During Continuous Cooling Transformation, *Heat Treat. Met.*, 2010, **35**(1), p 47–50 (in Chinese)
9. P. Deng, R.B. Song, T. Sun, and X. Wang, Continuous Cooling Transformation Diagram and Phase Transformation Model of 70Mn Steel, *Trans. Mater. Heat. Treat.*, 2014, **35**(4), p 208–212 (in Chinese)
10. T. Chen, C. Wu, A. Zhao, H. Zhao, X. Li, and S. Yao, Effects of Hardenability and Low Temperature Tempering Temperature on Microstructures and Properties of 60Si2CrA, *Hot. Working. Technol.*, 2016, 45(4), p 196–198, 201 (in Chinese)
11. Y. Jiang, Y.L. Liang, J. Xu, L. Lei, and M.G. Ou, Effect of Quenching Rate on Microstructure and Mechanical Properties of High Strength Spring Steel. *J. C. S. Univ. (Sci. Technol.)*, 2017, 48(3), p 617–624 (in Chinese)
12. M. Suehiro, T. Senuma, H. Yada, and K. Sato, Application of Mathematical Model for Predicting Microstructural Evolution to High Carbon Steels, *ISIJ Int.*, 1992, **32**(3), p 433–439
13. D. Quidort and Y.J.M. Brechet, A Model of Isothermal and Non Isothermal Transformation Kinetics of Bainite in 0.5% C Steels, *ISIJ Int.*, 2002, **42**(9), p 1010–1017
14. V. Colla, M. DeSanctis, A. Dimatteo, G. Lovicu, and R. Valentini, Prediction of Continuous Cooling Transformation Diagrams for Dual-Phase Steels from the Intercritical Region, *Metall. Mater. Trans. A*, 2011, **42**(9), p 2781–2793
15. D.J. Yang, L.X. Ning, J.G. Lin, and T.A. Dean, Phase Transformation Constitutive Equations During Continuous Cooling, *J. Mech. Eng.*, 2009, **45**(2), p 301–307 (in Chinese)
16. N. Li, J. Lin, T.A. Dean, D. Dry, and D. Balint, Materials Modelling for Selective Heating and Press Hardening of Boron Steel Panels with Graded Microstructures, in *11th International Conference on Technology of Plasticity*, Nagoya, Japan, Oct 19–24, 2014
17. M.S. Htun, S.T. Kyaw, and K.T. Lwin, Effect of Heat Treatment on Microstructures and Mechanical Properties of Spring Steel, *J. Met. Mater. Miner.*, 2008, **18**(2), p 191–197
18. Y. Mu, B. Wang, J. Zhou, X. Huang, and X. Li, Hot Stamping of Boron Steel Using Partition Heating for Tailored Properties: Experimental Trials and Numerical Analysis, *Metall. Mater. Trans. A*, 2017, **48**(11), p 5467–5479
19. R.P. Garrett, S. Xu, J. Lin, and T.A. Dean, A Model for Predicting Austenite to Bainite Phase Transformation in Producing Dual Phase Steels, *Int. J. Mach. Tool. Manuf.*, 2004, **44**(7–8), p 831–837
20. H. Huang, B. Wang, X. Tang, and J. Li, Modeling of Non-isothermal Austenite Formation in Spring Steel, *Metall. Mater. Trans. A*, 2017, **48**(12), p 5799–5804